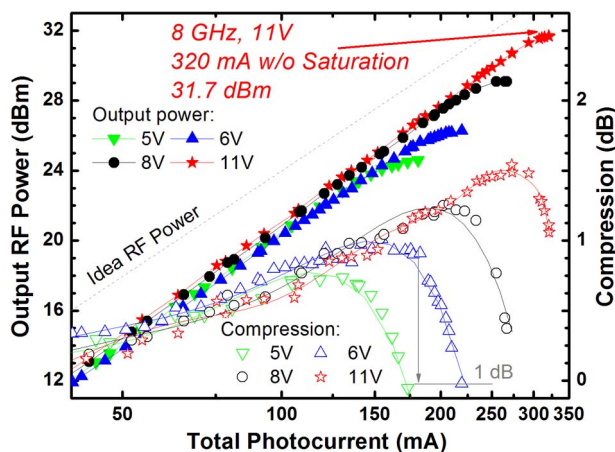


Balanced InP/InGaAs Photodiodes With 1.5-W Output Power

Volume 5, Number 3, June 2013

Qiugui Zhou
Allen S. Cross
Yang Fu
Andreas Beling
Brian M. Foley
Patrick E. Hopkins
Joe C. Campbell, Fellow, IEEE



DOI: 10.1109/JPHOT.2013.2262672
1943-0655/\$31.00 ©2013 IEEE

Balanced InP/InGaAs Photodiodes With 1.5-W Output Power

Qiugui Zhou,¹ Allen S. Cross,¹ Yang Fu,¹ Andreas Beling,¹ Brian M. Foley,²
Patrick E. Hopkins,² and Joe C. Campbell,¹ *Fellow, IEEE*

¹Department of Electrical and Computer Engineering, University of Virginia,
Charlottesville, VA 22904 USA

²Department of Mechanical and Aerospace Engineering, University of Virginia,
Charlottesville, VA 22904 USA

DOI: 10.1109/JPHOT.2013.2262672
1943-0655/\$31.00 © 2013 IEEE

Manuscript received March 23, 2013; revised April 25, 2013; accepted May 5, 2013. Date of publication May 16, 2013; date of current version May 29, 2013. This work was supported by the DARPA TROPHY program. P. E. H. is grateful for support from the AFOSR Young Investigator Program (FA9550-13-1-0067). Corresponding author: Q. Zhou (e-mail: qz6s@virginia.edu).

Abstract: We report InP/InGaAs modified unitraveling-carrier balanced photodiodes (PDs). The back-illuminated PDs were flip-chip bonded on diamond submounts for enhanced heat sinking. The device demonstrated a 3-dB bandwidth of 8 GHz and a 30-dB common-mode rejection ratio at frequencies of < 10 GHz. High saturation current of > 320 mA, maximum output power of 31.7 dBm (1.5 W) into a 50- Ω load, and good linearity with a third-order intercept point of up to 47 dBm were measured at the 3-dB bandwidth frequency of 8 GHz.

Index Terms: Photodiodes, photodetector.

1. Introduction

To enhance the signal-to-noise ratio and spur-free dynamic range, photodiodes (PDs) with large bandwidth, high power-handling capability, and high linearity have become key components in many analog photonic systems. High-power PDs also provide the option of using low-noise optical amplifiers instead of radio frequency (RF) postdetection electronic amplifiers.

The space charge screening effect is known to be a major contributor to the collapse of the electric field in the depletion region at high current and can significantly limit the power-handling capabilities of PDs. Various PD structures such as the partially depleted absorber [1], the dual-depletion region [2], and the unitraveling carrier (UTC) [3] have been developed to achieve high output power at high frequency. In UTC PDs, photons generate carriers in a thin undepleted absorber, and only the fast carriers (electrons for InP) are injected into and travel across the depleted drift layer. For example, the saturation drift velocity of electrons in InP at the electric field intensity of ~ 10 kV/cm is more than an order of magnitude larger than that of holes in $\text{In}_{0.48}\text{Ga}_{0.52}\text{As}$. Thus, compared with $\text{In}_{0.48}\text{Ga}_{0.52}\text{As}$ p-i-n PDs with the same depletion region width, the InGaAs/InP UTC PDs can have a much shorter transit time and reduced space charge screening at high current levels. To further enhance the performance of UTC PDs, several modifications including an additional thin depleted absorption layer [4] to increase responsivity, a cliff layer [5] to maintain high field in the undepleted absorber, and doping in the drift layer to “pre-tilt” the electric field to compensate the space charge [6] have been adopted. Charge-compensated modified UTC (CC-MUTC) PDs with a cliff layer, namely, UTC PDs incorporating these modifications, have been reported to have a high output power of 23.7 dBm and 18-GHz 3-dB bandwidth [7]. Increased maximum output power with reverse bias voltage was also observed for these devices,

but at high currents, the operation voltage was limited by thermal failure. It has been demonstrated that the power-handling capability of PDs can be increased by using an efficient heat sink [8] or flip-chip bonding the PDs on submounts with high thermal conductivity [9], [10].

Combining the photocurrent or output power from multiple PDs was studied as another option to achieve even greater power-handling capabilities. Compared with the other reported multiple-PD configurations, such as traveling-wave PD arrays [11] or power combiner PDs [12], balanced PDs [13] have the advantages of a relatively simple layout and direct summing of the current with negligible insertion loss. More importantly, the balanced-PD configuration can reduce system noise by suppressing the amplified spontaneous emission noise (ASE) from erbium-doped fiber amplifiers (EDFAs) and laser relative intensity noise (RIN) [13]. As a result, balanced PDs are favored for many photonic systems. Recently, Houtsma *et al.* have reported balanced UTC PDs with high output power of 1 W and 324 mW at 2 and 10 GHz, respectively [14].

In this paper, we report InP/InGaAs CC-MUTC balanced PDs with a cliff layer. The InP chip was flip-chip bonded on a chemical vapor deposition (CVD) diamond submount to improve heat dissipation. The balanced PDs exhibited 3-dB bandwidth of 8 GHz and a total photocurrent of 320 mA (160 mA on each PD) without reaching 1-dB compression saturation. The measured maximum output RF power at 8 GHz was 1.5 W. A three-tone intermodulation distortion measurement yielded a third-order intercept point (OIP3) of 47 dBm.

2. Experimental Details

2.1. Device Fabrication

The back-illuminated balanced PDs were fabricated from an InP/InGa_{0.47}As_{0.53} wafer with the same epitaxial layer design as the previously reported CC-MUTC PDs with a cliff layer [7]. The epitaxial layers were grown by metal-organic CVD. The layer configuration details are summarized in Table 1. A dry-etched double-mesa procedure was used to define the active area and isolate the PDs. Evaporating a Ti/Pt/Au metal stack formed both p- and n-metal contacts. The distance between the two diodes of the balanced pair was designed to be 250 μm to match the pitch of the fiber array. Au bonding bumps with diameter 6 μm smaller than that of the device active area and ~ 2 μm height were plated on both p and n contacts. A 250-nm-thick SiO₂ layer was deposited on the backside of the wafer as an antireflective (AR) coating, and the wafer was then diced into 1×1.3 mm² chips. Fig. 1(a) shows a scanning electron microscope (SEM) image of an InP chip with four balanced-PD pairs and two discrete PDs.

The thermal conductivity of the CVD diamond used for this work was measured by time-domain thermoreflectance to be > 500 W/m/K [15]. Fig. 1(b) is a photograph of a diamond submount with six sets of microwave pads corresponding to each PD or a balanced-PD pair on the InP chip. The black dashed lines indicate the position of the InP chip after flip-chip bonding. The pads were formed by Au plating, and the parts corresponding to the n-mesas on the chip were up plated to compensate the height of the p-mesa. A cross-sectional view of a flip-chip-bonded balanced-PD pair is depicted schematically in Fig. 1(c). The Joule heat generated in the p-n junction can be dissipated into the diamond submount through the plated Au bonding bumps and pads, as indicated by arrows in the figure.

2.2. Device Characterization

The responsivity, frequency response, and saturation current measurements were carried out with $\sim 100\%$ modulation depth generated by heterodyning two distributed-feedback laser diodes (LDs) near a 1550-nm wavelength, each of which is followed by a polarizer controller (PC). The beat frequency of the signal was controlled by adjusting the temperature of one of the LDs, thus slightly changing its wavelength. The heterodyne frequency was determined by monitoring one output arm of the 2×2 fiber coupler with a 50-GHz PD connected to a spectrum analyzer. The signal power of the second output arm was amplified by an EDFA and controlled by a variable optical attenuator (VOA). Subsequently, the signal was divided equally to feed the balanced pair of PDs via a lensed

TABLE 1

Epitaxial layer structure of CC-MUTC PDs with a cliff layer

| Layer | Material, doping and thickness |
|--------------------------------------|--|
| p-contact | InGaAs, 2.0×10^{19} Zn, 50nm (top layer) / InP, 1.5×10^{18} Zn, 100nm |
| grading layer | InGaAsP, Q1.1, 2.0×10^{18} Zn, 15nm / InGaAsP, Q1.4, 2.0×10^{18} Zn, 15nm |
| step-grade doped undepleted absorber | InGaAs, 2.0×10^{18} Zn, 100nm / InGaAs, 1.2×10^{18} Zn, 150nm / InGaAs, 8.0×10^{17} Zn, 200nm / InGaAs, 5.0×10^{17} Zn, 250nm |
| depleted absorber | InGaAs, 1.0×10^{16} Si, 150nm |
| grading layer | InGaAsP, Q1.4, 1.0×10^{16} Si, 15nm / InGaAsP, Q1.1, 1.0×10^{16} Si, 15nm |
| cliff layer | InP, 1.4×10^{17} Si, 50nm |
| charge compensated drift layer | InP, 1.0×10^{16} Si, 900nm |
| n-contact | InP, 1.0×10^{18} Si, 100nm / InP, 1.0×10^{19} Si, 900nm / InGaAs, 1.0×10^{19} Si, 20nm / InP, 1.0×10^{19} Si, 200nm |
| Substrate | InP, semi-insulating, double side polished |

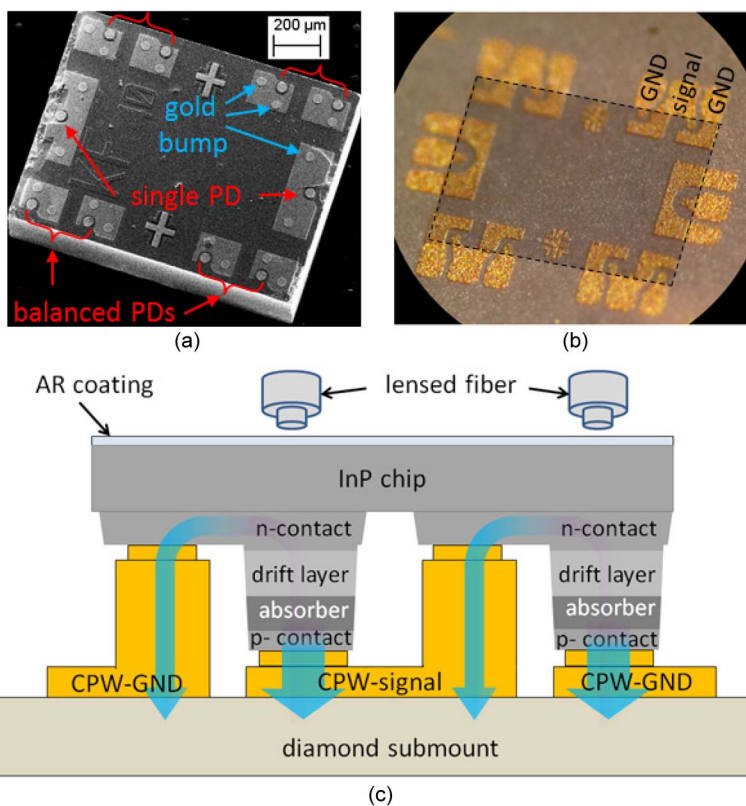


Fig. 1. (a) SEM image of an InP chip with four pairs of balanced PDs and two single PDs. (b) Photomicrograph of a diamond submount. (c) Schematic cross-sectional view of balanced PDs flip-chip bonded on a diamond submount. The blue arrows indicate the direction of heat flow.

fiber array. A variable optical delay line in one of the paths was used to control the modulation phase difference of the optical signal and switch between common mode, i.e., zero phase difference, and differential mode, i.e., phase difference of $(2n + 1)\pi$. The responsivity of these devices was measured to be 0.75 A/W. To attain uniform illumination of the PDs, the fibers were pulled back until the photoresponse dropped to half the peak value. The device under test was placed on a thermoelectric cooler with a surface temperature of ~ -10 °C. The PDs were biased separately by two dc source meters through bias-tees integrated on the microwave probe. The RF signal from the

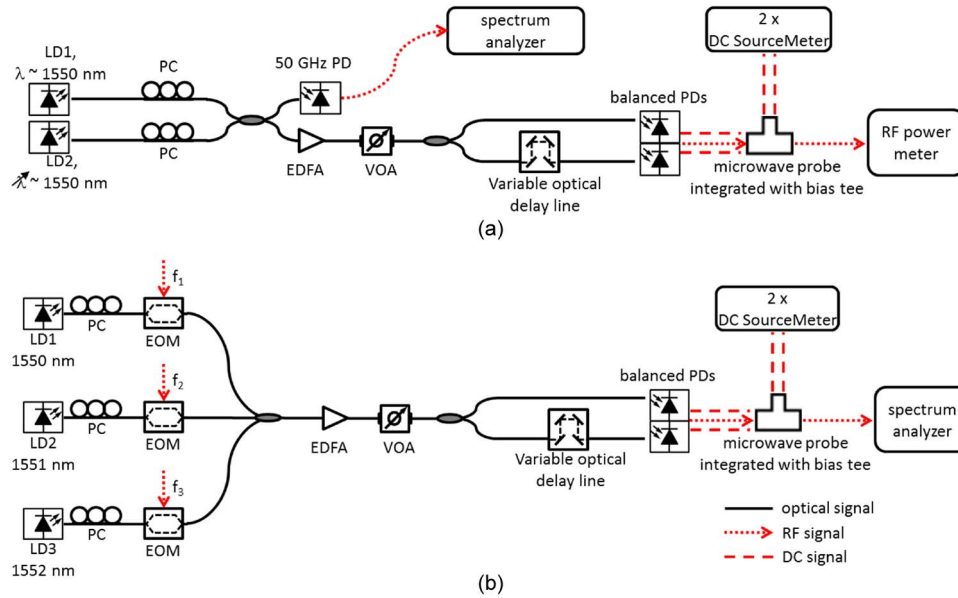


Fig. 2. (a) Heterodyne setup for bandwidth and saturation current measurements of balanced PDs. (b) Three-tone setup OIP3 measurement.

microwave probe was measured with a power meter. The measurement apparatus is depicted in Fig. 2(a). The compression measured at photocurrent I can be calculated using the expression

$$\text{Compression}(I) = [P_{\text{ideal}}(I_0) - P(I_0)] - [P_{\text{ideal}}(I) - P(I)] \quad (1)$$

where I_0 is a small current far below saturation, $P_{\text{ideal}}(I) = I^2 R/2$ is the ideal RF power on load R assuming 100% modulated current, and $P(I)$ is the measured output power from the PD(s) at I . All the device measurements described below were made with an output impedance of $R = 50 \Omega$. The current at which the compression drops 1 dB from its peak value is referred to as the saturation current.

A three-tone third-order intermodulation distortion (OIP3) measurement setup [15], as depicted in Fig. 3(b), was used for linearity characterization. Compared with a two-tone OIP3 setup, the three-tone setup possesses the advantage of being insensitive to harmonics of the light source; thus, the measurement would not be affected even if the modulators were biased off-quadrature [16]. The three tones were modulated at $f_1 = 8.0$ GHz, $f_2 = 7.9915$ GHz, and $f_3 = 7.998$ GHz through three high-speed Mach-Zehnder electrooptic modulators (EOMs). The OIP3 was calculated with

$$\text{OIP3} = \bar{P}_f + \frac{1}{2}(\bar{P}_f - \bar{P}_{\text{IMD3}}) + 3 \text{ dB} \quad (2)$$

where \bar{P}_f and \bar{P}_{IMD3} are the average power of the fundamental tone and the third-order intermodulation acquired from the spectrum analyzer, respectively. The 3 dB in (2) is added to convert the three-tone measurement result to an equivalent two-tone OIP3 since OIP3 values are conventionally reported in terms of two-tone measurement results.

3. Results

3.1. Bandwidth

The frequency response of the balanced PDs was measured at a reverse bias of 6 V. For single-diode illumination, when the optical signal was present on only one diode of the balanced pair, the device showed 3-dB bandwidth of 9 GHz at a photocurrent of 60 mA. As expected, this bandwidth is approximately half the bandwidth of a discrete single PD with the same diameter of 40 μm [7]. This

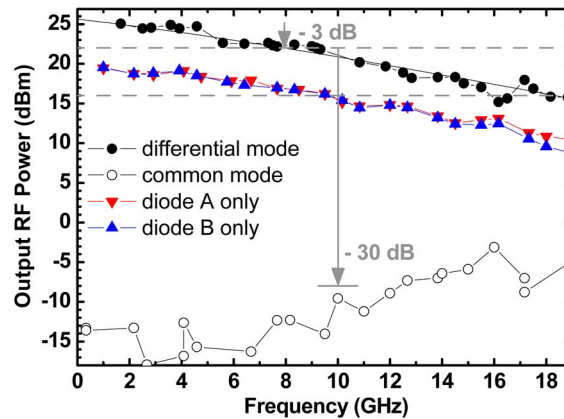


Fig. 3. Frequency responses of flip-chip-bonded balanced PDs at differential mode (\bullet), common mode (\circ), and with optical signal on only one device (\blacktriangledown and \blacktriangle).

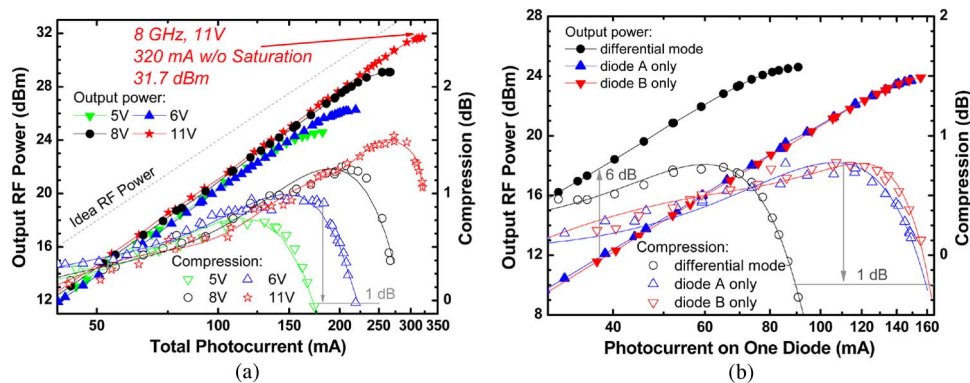


Fig. 4. (a) Saturation current of differential-mode balanced PDs measured at reverse bias voltages ranging from 5 to 11 V and a frequency of 8 GHz. (b) Saturation current of balanced PDs at differential mode and optical signal on only one PD at a reverse bias of 5 V.

is a direct result of the doubled capacitance in the balanced design since the bandwidth of these PDs is primarily RC limited. Compared with the single-diode illumination results, the differential measurement of the balanced pair with 60-mA photocurrent on both diodes showed an increase of approximately 6-dB RF output power and a 3-dB bandwidth of 8 GHz. The common-mode rejection ratio (CMRR), the ratio of the common-mode output RF power to the differential-mode output RF power, was close to 40 dB at low frequency and remained above 30 dB for frequencies up to 11 GHz. The CMRR continuously dropped as the frequency further increased, which agrees well with the increasing divergence of the RF responses of the two diodes under single-diode illumination, i.e., the separation between the line with “ \blacktriangle ” symbols and the line with “ \blacktriangledown ” symbols in Fig. 3.

3.2. Saturation Current

As shown in Fig. 4(a), the compression of the balanced PDs operating in differential mode initially increases slowly as the total photocurrent increases and then drops due to saturation. The super-linear increase in output RF power and the resulting increase in the compression with photocurrent have been previously reported for UTC-type PDs and explained in terms of a current-induced field in the absorber [7], [17]. The 1-dB compression point was measured at a total photocurrent of 180 mA (90 mA on each diode of the balanced pair) and output power of 24.6 dBm. The saturation current increases to 219 and 267 mA as the reverse bias increases to 6 and 8 V, respectively. At 11-V reverse bias voltage, the balanced PDs exhibit maximum output power of

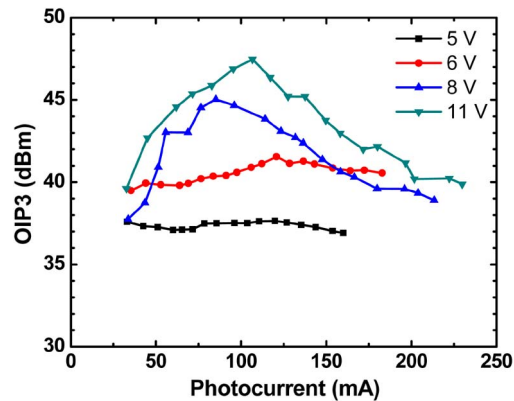


Fig. 5. Linearity of differential-mode balanced PDs.

31.7 dBm where the total photocurrent is 320 mA. The device is not saturated as the compression has dropped only 0.5 dB but further increase in the photocurrent is limited by the available optical power of our measuring setup.

Fig. 4(b) shows the saturation current and compression of the balanced PDs for the case that only one diode is illuminated together with measurements under differential mode. As was predicted by summing the photocurrents, the output RF power of the PD pair for differential-mode operation is ~ 6 dB higher than for single illumination with the same individual photocurrents until the current levels increased to ~ 60 mA where the differential-mode output power begins to be affected by saturation. The differential-mode compression decreases by 1 dB at 180 mA (90-mA photocurrent on each diode, or a saturation current density $J_{\text{sat}} = 7.2 \text{ kA/cm}^2$). When only one diode is illuminated, the compression peaks at ~ 110 mA and reaches 1-dB compression at 160 mA ($J_{\text{sat}} = 12.6 \text{ kA/cm}^2$). The large discrepancy between J_{sat} but similar total saturation currents for these two cases can be explained by the modulation of bias on the device due to the load voltage swing. The voltage drop across the p-n junction, V_{pn} , reaches the minimum point when the voltage swing on the $50\text{-}\Omega$ load peaks. At the 3-dB cutoff frequency, this voltage can be calculated using the following [6]:

$$\min(V_{\text{pn}}) = V_{\text{bi}} - V_{\text{bias}} - \frac{50I_{\text{ph}}}{\sqrt{2}} \quad (3)$$

where V_{bi} is the built-in voltage of the diode (approximately 0.8 V for these devices), and the bias voltage is V_{bias} , which was -5 V. The last term comes from the ac-voltage swing; I_{ph} is the total photocurrent. The minimal V_{pn} at the current where the compression peaks calculated with (3) is 1.5 and 1.8 V for the case of balanced differential mode and illumination of a single diode, respectively. As the current density is different for these two cases, the different space charge may explain the small discrepancy between the minimal voltage across the p-n junction. This low minimal V_{pn} at the current where the compression peaked could be attributed to the cliff layer and compensating charge in the drift layer, which diminished the space charge screening effect at a high current level. This also indicates that a good heat sink that enables operation at high reverse bias voltage to compensate the large voltage swing is critical for these devices to achieve high output power.

3.3. Linearity

The photocurrent dependence of OIP3 under reverse bias voltages in the range of 5–11 V at 8 GHz is shown in Fig. 5. At reverse bias voltages of 8 V or higher, significant OIP3 peaks were observed, which could be caused by the trough of third-order intermodulation distortion products resulting from the Franz–Keldysh effect [18]. At a reverse bias voltage of 11 V, OIP3 was higher than 40 dBm for total currents of up to 230 mA, and a peak value of ~ 47 dBm was measured at a total photocurrent of 106 mA. This is close to the previously reported OIP3 of 48 dBm on balanced PDs [14] but at a higher frequency of 8 GHz rather than 3 GHz.

4. Conclusion

We have demonstrated high power-handling capability using balanced CC-MUTC PDs with a cliff layer flip-chip bonded on diamond. With a bandwidth of 8 GHz, the devices exhibited a record-high RF output power of 1.5 W, an improvement of 50% relative to previously published output power of PDs with bandwidth in the gigahertz range. These devices also demonstrated high linearity and CMRR.

References

- [1] X. Li, N. Li, X. Zheng, S. Demiguel, J. C. Campbell, D. A. Tulchinsky, and K. J. Williams, "High-saturation-current InP–InGaAs photodiode with partially depleted absorber," *IEEE Photon. Technol. Lett.*, vol. 15, no. 9, pp. 1276–1278, Sep. 2003.
- [2] F. J. Effenberger and A. M. Joshi, "Ultrafast, dual-depletion region, InGaAs/InP pin detector," *J. Lightwave Technol.*, vol. 14, no. 8, pp. 1859–1864, Aug. 1996.
- [3] T. Ishibashi, N. Shimizu, S. Kodama, H. Ito, T. Nagatsuma, and T. Furuta, "Uni-traveling-carrier photodiodes," in *Proc. Tech. Dig. Ultrafast Electron. Optoelectron.*, 1997, pp. 83–87.
- [4] D. H. Jun, J. H. Jang, I. Adesida, and J. I. Song, "Improved efficiency–bandwidth product of modified uni-traveling carrier photodiode structures using an undoped photo-absorption layer," *Jpn. J. Appl. Phys.*, vol. 45, no. 4B, pp. 3475–3478, Apr. 2006.
- [5] N. Shimizu, N. Watanabe, T. Furuta, and T. Ishibashi, "InP–InGaAs uni-traveling-carrier photodiode with improved 3-dB bandwidth of over 150 GHz," *IEEE Photon. Technol. Lett.*, vol. 10, no. 3, pp. 412–414, Mar. 1998.
- [6] N. Li, X. Li, S. Demiguel, X. Zheng, J. C. Campbell, D. A. Tulchinsky, K. J. Williams, T. D. Isshiki, G. S. Kinsey, and R. Sudharsanan, "High-saturation-current charge-compensated InGaAs–InP uni-traveling-carrier photodiode," *IEEE Photon. Technol. Lett.*, vol. 16, no. 3, pp. 864–866, Mar. 2004.
- [7] Z. Li, H. Pan, H. Chen, A. Beling, and J. C. Campbell, "High-saturation-current modified uni-traveling-carrier photodiode with cliff layer," *IEEE J. Quantum Electron.*, vol. 46, no. 5, pp. 626–632, May 2010.
- [8] N. Duan, X. Wang, N. Li, H. D. Liu, and J. C. Campbell, "Thermal analysis of high-power InGaAs–InP photodiodes," *IEEE J. Quantum Electron.*, vol. 42, no. 12, pp. 1255–1258, Dec. 2006.
- [9] Z. Li, Y. Fu, M. Piels, H. Pan, A. Beling, J. E. Bowers, and J. C. Campbell, "High-power high-linearity flip-chip bonded modified uni-traveling carrier photodiode," *Opt. Exp.*, vol. 19, no. 26, pp. B385–B390, Dec. 2011.
- [10] Q. Zhou, A. Cross, Y. Fu, A. Beling, and J. C. Campbell, "High-power high-bandwidth flip-chip bonded modified uni-traveling carrier photodiodes," in *Proc. IEEE IPC*, 2012, pp. 306–307.
- [11] A. S. Cross, Q. Zhou, A. Beling, Y. Fu, and J. C. Campbell, "High power flip-chip mounted traveling wave detector," *Opt. Exp.*, vol. 21, no. 8, pp. 9967–9973, Apr. 2013.
- [12] Y. Fu, H. Pan, and J. C. Campbell, "Photodiodes with monolithically integrated Wilkinson power combiner," *IEEE J. Quantum Electron.*, vol. 46, no. 4, pp. 541–545, Apr. 2010.
- [13] M. S. Islam, T. Jung, T. Itoh, M. C. Wu, A. Nespola, D. L. Sivco, and A. Y. Cho, "High power and highly linear monolithically integrated distributed balanced photodetectors," *J. Lightwave Technol.*, vol. 20, no. 2, pp. 285–295, Feb. 2002.
- [14] V. E. Houtsmma, T. Hu, N. Weimann, R. Kopf, A. Tate, J. Frackoviak, R. Reyes, Y. Chen, and L. Zhang, "A 1 W linear high-power InP balanced uni-traveling carrier photodetector," in *Proc. Eur. Conf. Expo. Opt. Commun.*, 2011, pp. 1–3.
- [15] H. Pan, Z. Li, A. Beling, and J. C. Campbell, "Characterization of high-linearity modified uni-traveling carrier photodiodes using three-tone and bias modulation techniques," *J. Lightwave Technol.*, vol. 28, no. 9, pp. 1316–1322, May 2010.
- [16] T. Ohno, H. Fukano, Y. Muramoto, T. Ishibashi, T. Yoshimatsu, and Y. Doi, "Measurement of intermodulation distortion in a unitraveling-carrier refracting-facet photodiode and a p–i–n refracting-facet photodiode," *IEEE Photon. Technol. Lett.*, vol. 14, no. 3, pp. 375–377, Mar. 2002.
- [17] H. Ito, S. Kodama, Y. Muramoto, T. Furuta, T. Nagatsuma, and T. Ishibashi, "High-speed and high-output InP–InGaAs unitraveling-carrier photodiodes," *IEEE J. Sel. Topics Quantum Electron.*, vol. 10, no. 4, pp. 709–727, Jul./Aug. 2004.
- [18] A. Beling, H. Pan, H. Chen, J. Campbell, A. Hastings, D. Tulchinsky, and K. Williams, "Impact of voltage-dependent responsivity on photodiode non-linearity," in *Proc. IEEE 21st Annu. Meeting LEOS*, 2008, pp. 157–158.